Indian Journal of Ecology (2024) 51(2): 258-265
DOI: https://doi.org/10.55362/IJE/2024/4227

Manuscript Number: 4227
NAAS Rating: 5.38

Spatio-Temporal Changes of Water Bodies using Spectral Indices in AABR, Chhattisgarh, Central India

Gayatri Devi and S.C. Tiwari

Department of Forestry, Wildlife and Environmental Sciences
Guru Ghasidas Central University, Bilaspur, Chhattisgarh-495 009, India
E-mail: gayatrikushwaha336@gmail.com

Abstract**:** The possibility of an ecological imbalance in forests has been pointed up because of the decreasing amount of water source in a forested area**.** Central Indian land receives an abundant but uneven spatiotemporal distribution of rainfall and has evident seasonal water shortages. Remote sensing and GIS techniques are employed for locating and monitoring water bodies, intended to highlight spatio-temporal change patterns of surface water bodies in the protected region of Achanakmar-Amarkantak Biosphere Reserve (AABR) from 2000 to 2020. However, Multi-temporal Landsat satellite data is thoroughly examined through the application of a spectral water indexing method. This method involves leveraging specific spectral bands Near infrared (NIR) and Shortwave infrared (SWIR) that are sensitive to the presence of water, allowing for the precise identification and mapping of water bodies over the study time periods. In study used water indices, Normalized Difference Water Index (NDWI), and Modified Normalized Difference Water Index (MNDWI) to provide significant results for extracting surface water bodies and finding out spatio-temporal changes patterns of the water bodies. The NDWI was employed for assessing the spatial extent of water bodies in the year 2000, revealing a water area of 7.0 km² during pre-monsoon and 32.4 km² for post-monsoon periods, while in 2020, the water area was measured at 22.0 km² in the pre-monsoon season and 50.9 km² in the post-monsoon season. Additionally, MNDWI) was utilized to estimate surface water body extent, indicating a water area of 8.3 km² in the pre-monsoon season and 42.1 km² in the post-monsoon season for the year 2000. In 2020, the water area was measured at 27.0 km² in the pre-monsoon season and 52.3 km² in the post-monsoon season. The monitoring of the AABR is imperative for detecting changes in the area of its surface water bodies that have transpired in recent years. This approach proves highly effective for monitoring and analyzing spatio-temporal variations in water bodies, significantly enhancing our comprehension of landscape dynamics and environmental changes.

Keywords: NDWI, MNDWI, AABR, Geoinformatics, Water bodies, Spectral indices

Water is crucial to the creation of life and the development of human civilization (Falkenmark 2020, Bulavin et al 2020). The water bodies on the surface of the earth have seen significant changes as a consequence of the changing global climate and increased human activities (Tao et al 2011, Yang et al 2015). However freshwater represents only 3% of existing water on the planet, of which 0.3% is available for humans (McDonald et al 2011). On Earth, there are various forms of water, including surface water, groundwater, aquifers, coastal water, and inland water (Oki 2020). Water security and accessibility are important factors for both living organisms and natural ecosystems worldwide (Haddeland et al 2014, Gril et al 2019, Krause et al 2020). Therefore, modern techniques of remote sensing and geographic information systems facilitate the detection and monitoring of water bodies in various regions of the world without making direct contact (Lasaponara et al 2012, Opolot 2013). The signature radiation of each object on the Earth's surface that distinguishes it from others is known as the reflectance band. Remote sensing and geographic information systems employ reflectance bands to analyze the geographic components (Pekel et al 2016, Donchyts et al 2016). The optical sensor and the microwave sensor can be utilized to measure surface water (Watts et al 2012, Schroeder et al 20015, Huang et al 2016). Microwave sensors have the ability to penetrate cloud coverage and certain vegetation coverage due to their usage of long-wavelength radiation (Shrestha et al 2019). There are many natural and man-made reasons, surface water bodies are dynamic in nature and fluctuate in size, shape, appearance, and flow over time (Karpatne et al 2016, Pekel et al 2016). Optical sensors have been widely used in this field due to high data availability, as well as suitable spatial and temporal resolutions (Bhavsar 1984, Huang et al 2015). Normalized difference vegetation index (NDVI) categorizes floods and surface water (Fu et al 2015). Normalized difference water index (NDWI) makes use of reflected near-infrared radiation and visible green light to enhance the presence of such features while eliminating the presence of soil and terrestrial vegetation features (Xu et al 2006). There was extensive usage in the first ten years of the twenty-first century (Nandi et al 2018, Wang et al 2020, Li et al 2022), and modified normalized difference water index

(MNDWI) have been the most useful indices to identify waterbodies and their surface-water spread over the years (Acharya et al 2006). Many researchers have reported the use of NDWI and MNDWI for surface water monitoring (Du et al 2012, Gautam et al 2015, Buma et al 2018, Sekertekin et al 2018, Masocha et al 2018, Ali et al 2019, Bhangale et al 2020, Rad et al 2021, Dastour et al 2022). Remote sensing has developed techniques to change spatio-temporal attributes in georeferenced imagery for extraction of water pixels (Wadhwa et al 2018). Normalized Difference Water Index (NDWI) was applied to classify land and water components from satellite images for automatically extracting the coastline of Diu Island, India (Pham et al 2018). Water body extraction is an important undertaking in different fields. This paper detected the spatiotemporal changes in water bodies in AABR.

MATERIAL AND METHODS

Study area: Achanakmar-Amarkantak biosphere reserve is named after Achanakmar forest village and Amarkantak, from where the rivers Narmada, Johilla, and Sone emerge. Achanakmar-Amarkantak Biosphere Reserve was declared a Biosphere Reserve (BR) by the Government of India in 2005. It falls in tropical dry deciduous forest biomes. Vegetation is generally tropical moist deciduous forests and tropical dry deciduous forests with grassland areas. It lies between latitude 22° 15'N to 21° 58'N and longitude 81° 25'E to 82° 5'E. The total geographical area of AABR is 3835.51 km^2. hosting about 418 villages and 436128 tribal populations inside the AABR (Roychoudhury et al 2020). Daily maximum temperature ranges from 10 °C to 39 °C depending upon season and rainfall. The Biosphere Reserve spreads over 3835.51 sq. km (2610.53 sq. km in Chhattisgarh and 1224.94 sq. km in Madhya Pradesh).

Data description: For the analysis of surface water of the Achanakmar-Amarkantak biosphere reserve (AABR), GEE a web-based cloud computing platform that provides over 11 petabytes of earth observation data was used. GEE offers various advantages-access to the large volume of processed remote sensing image data and dedicated cloud storage; simple and rapid programming and graphic interface and the possibility for assessing surface water dynamics at the planetary scale for a prolonged period. Landsat 5, 7, and 8 with 30 m resolution data were acquired in the pre-monsoon and post-monsoon seasons for the periods 2000, 2010, and 2020 in the study area following the United States Geological Survey (USGS) (Table 1). Five Landsat 5 Thematic Mapper (TM), two Landsat 7 Enhanced Thematic Mapper Plus (ETM+), and eight Landsat 8 Operational Land Imager (OLI)/Thermal Infrared Sensors (TIRS) data of pre-monsoon seasons and post-monsoon seasons were freely obtained from the GEE.

Normalized difference water index (NDWI): The normalized difference water index (NDWI) is a new method that defines the features of open water and enhances its presence and visibility in remotely sensed digital images (Li et al 2013, Gao 1996). NDWI method uses reflected radiation in the visible green light and near-infrared bands as shown in eq. 1 (Mcfeeters 1996):

NDWI = (Green – NIR)/ (Green + NIR).....(eq.1)

Where NIR is Near-infrared, NDWI value ranges from -1.0 to 1.0. The positive values represent water area whereas the negative values represent non-water lands (Mcfeeters 1996).

Modified normalized differences water index (MNDWI): The MNDWI technique is almost similar to NDWI with only one exception of using a middle infrared band instead of a near-infrared band. This is simply a masking procedure that separates the land. Primarily, it is used for the removal of built-up land noise. In the MNDWI method, the water areas possess higher pixel values as compared to urban or vegetation areas with lower pixel values. Therefore, it delineates the water class from other classes. This method can also efficiently eliminate shadow noise from the water data without involving advanced procedures (Han 2005). The replacement of near-infrared band in NDWI with visible green light and middle infrared bands (MIR) in MNDWI occurs as shown in eq. 2 (Xu 2006):

MNDWI = (Green – MIR)/ (Green + MIR).....(eq.2)

RESULTS AND DISCUSSION

The images given below, which was acquired from the field changes in the AABR from (Fig. 2a-c) pre-monsoon (may) and (Fig. 2d-f) post-monsoon (November) in 2023. The water indices revealed fluctuating and variable threshold values according to the type of water indices and time intervals (Mashagbah et al 2021). The water pixels are known to have positive values whereas other land cover areas exhibit zero or lower values (Yang et al 2017). The NDWI and MNDWI-based water threshold values were observed to be generally greater than 0.3.

Water bodies change analysis based on NDWI: NDWI index is used to emphasize the reflectance of water by using a green band, and suppress the low reflectance of NIR by water features. NDWI indices on pre-monsoon ETM+ (year 2000) recorded water area of 7.0 Km^2 and land area of 3935 Km^2. Similarly in post-monsoon water area is 32.4 Km^2 and the land area is 3909.6 Km^2. In 2010 TM images water area of 12.3 km^2 and land area is 3929.6 km^2 (Table 2, Fig. 3). Similarly in post-monsoon water area is 27 km^2 and the land

Table 1. Specifications of satellite data used in the present study

Year	Satellite/Sensor	Spectral bands(μm)	Spatial resolution (m)	Source of data
2000	Landsat-7 ETM+	Band 1: 0.452–0.514	30	USGS Website
		Band 2: 0.519–0.601	30	
		Band 3: 0.631–0.692	30	
		Band 4: 0.772–0.898	30	
		Band 5: 1.547–1.748	30	
		Band 6: 10.31–12.36	30	
		Band 7: 2.065–2.346	30	
		Band 8: 0.515–0.896	15	
2010	Landsat-5 TM	Band 1: 0.452-0.518	30	USGS Website
		Band 2: 0.528-0.609	30	
		Band 3: 0.626-0.693	30	
		Band 4: 0.776-0.904	30	
		Band 5: 1.567-1.784	30	
		Band 6: 10.40-12.50	120	
		Band 7: 2.097-2.349	30	
2020	Landsat- 8 OLI	Band 1: 0.43-0.45	30	USGS Website
		Band 2: 0.45-0.51	30	
		Band 3: 0.53-0.59	30	
		Band 4: 0.64-0.67	30	
		Band 5: 0.85-0.88	30	
		Band 6: 1.57-1.65	30	
		Band 7: 2.11-2.29	30	
		Band 8: 0.50-0.68	15	
		Band 9: 1.36-1.38	30	
2000-2020	IMD Precipitation	1.0 x 1.0 degree (Grided data)		IMD

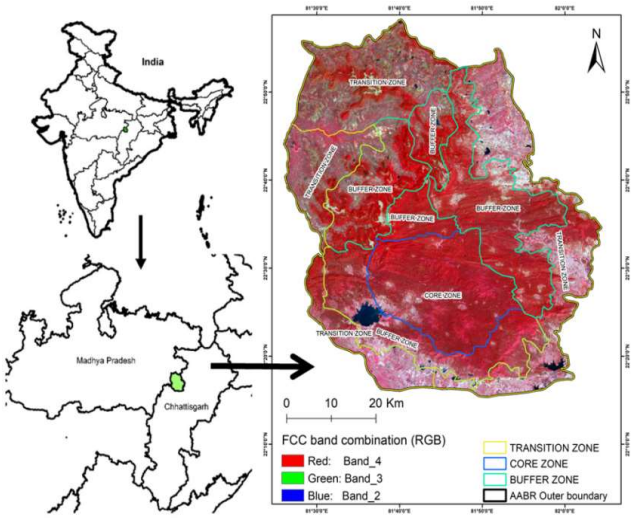

Fig. 1. Location of the study area, a standard false color composite (FCC) of Landsat- 8 OLI

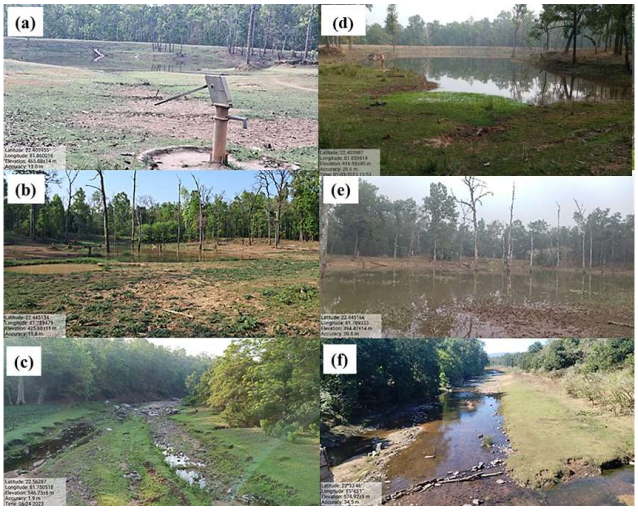

Fig. 2. Delineation of water bodies in AABR, (a-c) pre-monsoon (May), and (d-f) post-monsoon (November) in the AABR range

area is 3915 km^2. The examination of Operational Land Imager (OLI) images in 2020 unravels increase in water area, with NDWI revealing a water extent of 22 km^2 during the pre-monsoon season and land area is 3919.9 km^2. This substantial rise in water area likely signifies shifts in hydrological patterns, land use changes, or other environmental factors (Wagner et al 2016). The post-monsoon phase of 2020 continues to demonstrate this trend, with a water area of 50.9 Km^2 and the land area is 38893 km2 (Table 2). Comparing these findings across the years, study area's water bodies exhibit variability in response to annual climatic fluctuations. The post-monsoon periods consistently portray elevated water areas, indicative of the pivotal role played by the monsoonal rains in replenishing and expanding surface water bodies. Additionally, the varying magnitudes of water extent across different years underscore the dynamic nature of water systems, which can be influenced by a multitude of factors including precipitation patterns, land use changes, and anthropogenic activities (Van der Esch et al 2017). The NDWI-based assessments provide valuable information for understanding the interplay between climatic variations and surface water dynamics (Table 2, Fig. 3). These results contribute to a broader comprehension of hydrological processes within the study area and serve as a foundation for informed water resource management and environmental planning (Badham et al 2019). The consistency of NDWI in detecting water bodies across the years, despite their differing magnitudes, attests to the index's effectiveness in capturing water-related changes. However, it's important to note that further investigations into the underlying drivers of these changes, beyond the scope of this study, could shed additional light on the complex interactions shaping the observed patterns.

Water bodies change analysis based on MNDWI: Examining the results from the pre-monsoon period of 2000, the MNDWI-based assessment reveals a water area of approximately 8.3 km^2. This finding underscores the sensitivity of the MNDWI index in detecting even relatively modest water extents during periods of potentially lower water availability. The associated land area of 3933.7 km^2 provides context, illustrating the distribution of terrestrial features within the study area during this specific time frame. Transitioning to the post-monsoon phase of 2000, the MNDWI analysis shows a substantial expansion of water coverage, spanning about 42.1 km^2. This considerable increase underscores the considerable impact of seasonal variations, particularly monsoonal precipitation, on the augmentation of surface water bodies. The concurrent decrease in land area to 3899.8 km^2 further emphasizes the dynamic nature of these changes, wherein the land-water balance responds to meteorological influences. Turning to the year 2010 and the Landsat Thematic Mapper (TM) images, the pre-monsoon MNDWI assessment discloses a water area of approximately 14.4 km^2. This observation reaffirms the MNDWI's ability to capture water bodies, even during seasons with potentially less pronounced water features. The associated land area of 3927.6 km^2 offers a comprehensive view of the land-water distribution, indicating the composition of the study area during the pre-monsoon phase of 2010. The post-monsoon phase of 2010

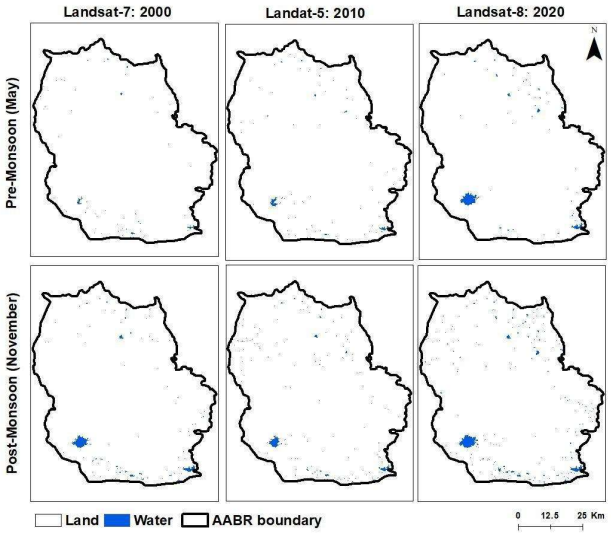

Fig. 3. Water bodies change pattern based on NDWI of Landsat data Pre and Post Monsoon (2000-2020)

Table 2. Water changes status based on NDWI (area in Km^2)

Year	Class	Pre-Monsoon	Post-Monsoon	Change (post-pre)
2000	Land	3935	3909.6	-25.4
	Water	7	32.4	25.4
2010	Land	3929.6	3915	-14.6
	Water	12.3	27	14.7
2020	Land	3919.9	3889.3	-30.6
	Water	22	50.9	28.9

underscores the index's responsiveness to seasonal shifts, showcasing a water area of 25.3 km^2 and a corresponding land area of 3916.7 km^2. The observed changes in water and land extent reveal the intricate interplay between hydrological variations and terrestrial elements. Fast-forwarding to the year 2020 and the use of Operational Land Imager (OLI) images, the pre-monsoon MNDWI assessment demonstrates a considerable water area of 27.0 km^2, suggesting pronounced water features during this time frame. The associated land area of 3915.0 km^2 provides context to the water extent, signifying the intricate relationship between land and water elements. Continuing the trend, the post-monsoon period of 2020 maintains the observed pattern, registering a water area of 52.3 km^2 and a corresponding land area of 3889.3 km^2 (Table 3). These consistent findings across various years underscore the reliability of MNDWI in capturing and quantifying changes in surface water dynamics.

Precipitation trends over water bodies: AABR has a tropical monsoon climate characterized by hot, humid, rainy summer, because of its proximity to the Tropic of Cancer and its dependence on the monsoons for rains. The monsoon season is from late June to October and winter. The annual average minimum, mean, and maximum temperatures in the area are 22˚C, 26˚C, and 33˚C, respectively. In the wet season, rainfall varies greatly and is influenced by local and regional hydroclimatic conditions. The area receives rainfall from South-West Monsoon. A broad variation of precipitation intensity characterizes the hot and muggy summer season. Local long-term rainfall varies greatly from month to month within a year. However, specific months show a wide range of rainfall variation across different years (Table 4). Overall, the hydrologic regime in the area is divided into dry (November through May) and wet seasons (June through October) (Fig. 5a, b). The wet season receives around 75% of the annual

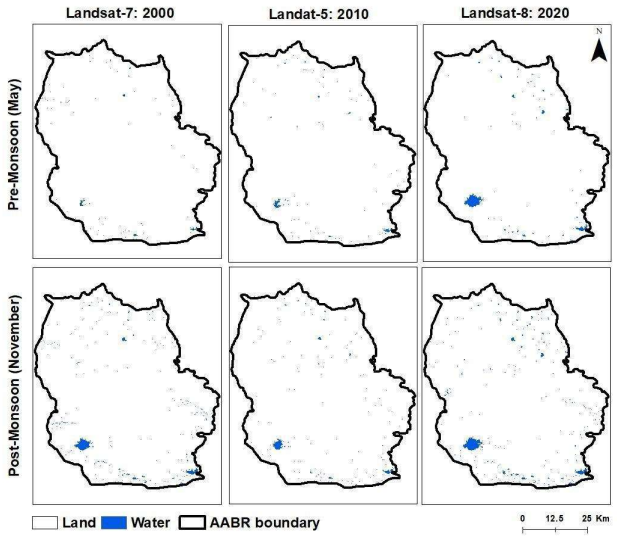

Fig. 4. Water bodies change pattern based on MNDWI of Landsat data Pre and Post Monsoon (2000-2020)

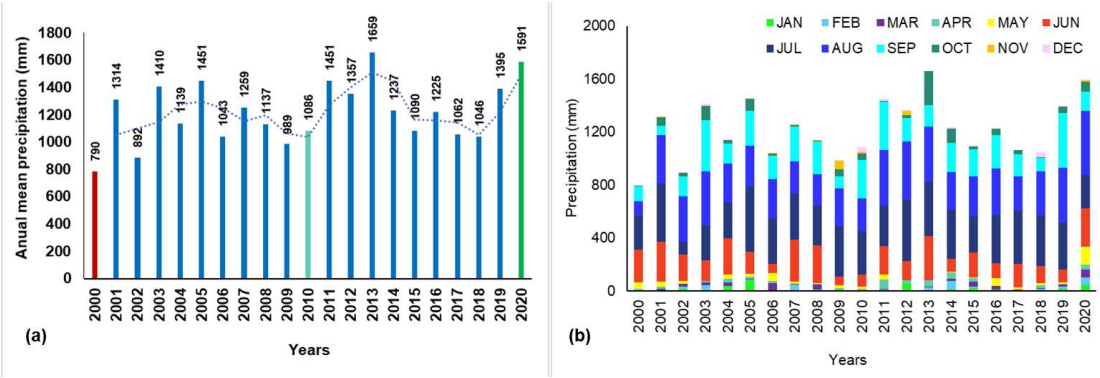

Fig. 5. (a) 20-year precipitation trends (Red: low precipitation in 2000, Yellow: moderate precipitation in 2010, and high precipitation in 2020) (b) monthly precipitation trends over water bodies in the AABR region

Table 3. Water changes status based on MNDWI (Area in Km^2)

Year	Class	Pre-Monsoon	Post-Monsoon	Change (post-pre)
2000	Land	3933.7	3899.8	-33.9
	Water	8.3	42.1	33.8
2010	Land	3927.6	3916.7	-10.9
	Water	14.4	25.3	10.9
2020	Land	3915	3888.0	-27
	Water	27	52.3	25.3

Table 4. Twenty years mean precipitation of AABR region

Month/ Year	January	February	March	April	May	June	July	August	September	October	November	December	Annual
2000	4	11	0	0	52	242	261	106	114	0	0	0	790
2001	3	0	13	19	34	301	440	364	74	66	1	0	1314
2002	17	12	22	0	25	196	97	343	151	26	0	0	892
2003	1	40	25	10	0	153	263	409	385	111	0	13	1410
2004	40	0	22	28	32	274	270	294	150	25	1	1	1139
2005	83	1	7	18	22	165	493	306	266	88	0	2	1451
2006	0	0	59	16	60	67	348	293	175	20	5	0	1043
2007	0	47	6	2	17	316	347	240	262	13	8	0	1259
2008	5	7	35	6	4	287	299	239	244	9	3	0	1137
2009	13	0	0	9	23	63	381	284	93	55	61	8	989
2010	7	0	0	9	13	96	328	243	291	50	14	37	1086
2011	0	10	4	70	41	214	305	417	368	2	0	19	1451
2012	58	10	0	11	3	143	464	438	181	20	30	0	1357
2013	0	25	9	45	1	332	409	422	160	257	0	0	1659
2014	8	64	21	46	7	95	372	283	218	107	0	15	1237
2015	24	7	38	27	4	191	275	296	207	18	0	2	1090
2016	10	3	25	2	54	116	366	347	252	49	0	0	1225
2017	2	5	4	0	15	177	405	255	167	31	0	0	1062
2018	0	19	1	21	19	130	381	331	104	3	0	38	1046
2019	17	12	20	5	8	97	357	411	413	48	0	7	1395
2020	41	61	61	35	132	294	250	484	142	77	11	1	1591

precipitation, which is brought on by tropical monsoon systems and convective rains.

Rainfall distribution with a long-term total annual average of 790 mm in 2000, and 1086 in 2010 and it has increased to 1591 mm in 2020 (Table 4). Thematic maps of pre-monsoon and post-monsoon **(**Fig. 3, 4) are correlated with rainfall. The water spread after the monsoon is larger as a result of the increased water release from the Maniyari River and Khudia Dams, as well as rains from the region below the dams through Feeder Rivers.

CONCLUSION

The surface water area in AABR was examined using geographic information systems and remote sensing methods to determine changes over time. The establishment of threshold values has emerged as a pivotal technique for delineating water bodies, offering a dynamic framework that adapts to the evolving nature of the region's hydroclimatic conditions. This adaptability has been demonstrated vividly through the varying threshold values observed across different time periods and in relation to the specific water indices employed. These nuanced threshold variations, in conjunction with the machine learning algorithm employed, have facilitated a robust estimation of surface water spread across the years 2000, 2010, and 2020, as derived from the Google Earth Engine (GEE). Water bodies have grown and expanded between 2000 and 2020, however, there is still a need for conserving water for the animals in certain areas. The findings of this study reverberate with implications for environmental management and conservation efforts.

ACKNOWLEDGMENTS

The authors are highly thankful to the Forest Department of Chhattisgarh for providing the necessary support during the field visit. Authors are also thankful to the satellite data provider USGS.

REFERENCES

Acharya TD, Subedi A and Lee DH 2018. Evaluation of water indices for surface water extraction in a Landsat 8 scene of Nepal. *Sensors* **18**(8): 1-15.

Al-Mashagbah AF, Ibrahim M and Al-Fugara A 2021. Estimation of changes in the Dead Sea surface water area through multiple water index algorithms and geospatial techniques. *Global Nest Journal* **23**(4): 565-571.

Ali MI, Dirawan GD Hasim AH and Abidin MR 2019. Detection of changes in surface water bodies urban area with NDWI and MNDWI methods. *International Journal on Advanced Science Engineering Information Technology* **9**(3): 946-951.

Badham J, Elsawah S, Guillaume JH, Hamilton SH, Hunt RJ, Jakeman AJ and Bammer G 2019. Effective modeling for Integrated Water Resource Management: A guide to contextual practices by phases and steps and future opportunities. *Environmental Modelling & Software* **116**: 40-56.

Bhangale U, More S, Shaikh T, Patil S, and More N 2020. Analysis of surface water resources using Sentinel-2 imagery. *Procedia Computer Science* **171**: 2645-2654.

Bhavsar PD 1984. Review of remote sensing applications in hydrology and water resources management in India. *Advances in Space Research* **4**(11): 193-200.

Bulavin LA, Gotsulskyi VY, Malomuzh NP and Fisenko AI 2020. Crucial role of water in the formation of basic properties of living matter. *Ukrainian Journal of Physics* **65**(9): 794-794.

Buma WG, Lee SI and Seo JY 2018. Recent surface water extent of Lake Chad from multispectral sensors and grace. *Sensors* **18**(7): 1-24.

Dastour H, Ghaderpour E and Hassan QK 2022. A combined approach for monitoring monthly surface water/ice dynamics of Lesser Slave Lake via Earth observation data. *IEEE Journal of Selected Topics in Applied Earth Observations and Remote Sensing* **15**: 6402-6417.

Donchyts G, Baart F, Winsemius H, Gorelick N, Kwadijk J and Van de Giesen N 2016. Earth's surface water change over the past 30 years. *Nature Climate Change* **6**(9): 810-813.

Du Z, Linghu B, Ling F, Li W, Tian W, Wang H and Zhang X 2012. Estimating surface water area changes using time-series Landsat data in the Qingjiang River Basin, China. *Journal of Applied Remote Sensing* **6**(1): 1-16

Falkenmark M 2020. Water resilience and human life support-global outlook for the next half century. *International Journal of Water Resources Development* **36** (2-3): 377–396.

Fu B and Burgher I 2015. Riparian vegetation NDVI dynamics and its relationship with climate, surface water and groundwater. *Journal of Arid Environments* **113**: 59-68.

Gautam VK, Gaurav PK, Murugan P and Annadurai MJAP 2015. Assessment of surface water dynamics in Bangalore using WRI, NDWI, MNDWI, supervised classification and KT transformation. *Aquatic Procedia* **4**: 739-746.

Grill G, Lehner B, Thieme M, Geenen B, Tickner D, Antonelli F and Zarfl C 2019. Mapping the world's free-flowing rivers. *Nature* **569**(7755): 215-221.

Haddeland I, Heinke J, Biemans H, Eisner S, Flörke M, Hanasaki N and Wisser D 2014. Global water resources affected by human interventions and climate change. *Proceedings of the National Academy of Sciences* **111**(9): 3251-3256.

Huang C, Chen Y, Wu J, Li L and Liu R 2015. An evaluation of Suomi NPP-VIIRS data for surface water detection. *Remote Sensing Letters* **6**(2): 155-164.

Huang C, Chen Y, Zhang S and Wu J 2018. Detecting, extracting, and monitoring surface water from space using optical sensors: A review. *Reviews of Geophysics* **56**(2): 333-360.

Karpatne A, Khandelwal A, Chen X, Mithal V, Faghmous J and Kumar V 2016. Global monitoring of inland water dynamics: State-of-the-art, challenges, and opportunities. *Computational sustainability* **645**: 121-147.

Krause CE, Newey V, Alger MJ and Lymburner L 2021. Mapping and monitoring the multi-decadal dynamics of Australia's open waterbodies using Landsat. *Remote Sensing* **13**(8): 1437.

Lasaponara R, Danese M and Masini N 2012. Satellite-Based Monitoring of Archaeological Looting in Peru, pp 177-193. In: Lasaponara, R., Masini, N. (eds) Satellite Remote Sensing. *Remote Sensing and Digital Image Processing,* vol 16. Springer, Dordrecht.

Li J, Ma R, Cao Z, Xue K, Xiong J, Hu M and Feng X 2022. Satellite detection of surface water extent: A review of methodology. *Water* **14**(7): 2-18.

Masocha M, Dube T, Makore M, Shekede MD and Funani J 2018. Surface water bodies mapping in Zimbabwe using landsat 8 OLI multispectral imagery: A comparison of multiple water indices. *Physics and Chemistry of the Earth, Parts a/b/c* **106**: 63-67.

McDonald RI, Green P, Balk D, Fekete BM, Revenga C, Todd M and Montgomery M 2011. Urban growth, climate change, and freshwater availability. *Proceedings of the National Academy of Sciences* **108**(15): 6312-6317.

McFeeters SK 1996. The use of the Normalized Difference Water Index (NDWI) in the delineation of open water features. *International journal of remote sensing* **17**(7): 1425-1432.

Nandi D, Chowdhury R, Mohapatra J, Mohanta K and Ray D 2018. Automatic delineation of water bodies using multiple spectral indices. *International Journal of Scientific Research in Science, Engineering and Technology* **4**(4): 498-512.

Oki T 2020. Hydrosphere-The water realm which supports human life, pp 39-46. In: Himiyama Y, Satake K, Oki T (eds) *Human Geoscience*. Advances in Geological Science. Springer, Singapore.

Opolot E 2013. Application of remote sensing and geographical information systems in flood management: a review. *Research Journal of Applied Sciences Engineering and Technology* **6**(10): 1884-1894.

Pekel JF, Cottam A, Gorelick N and Belward AS 2016. High-resolution mapping of global surface water and its long-term changes. *Nature* **342**: 850-853.

Pham BT and Prakash I 2018. Application of simple remote sensing techniques for the detection and extraction of coastline - A case study of Diu Island, India. *Indian Journal of Ecology* **45**(4): 778-784.

Rad AM, Kreitler J and Sadegh M 2021. Augmented normalized difference water index for improved surface water monitoring. *Environmental Modelling & Software* **140**(1): 1-15.

Roychoudhury N, Sharma R, Yadav DK and Kushwaha DK 2020. Achanakmar-Amarkantak biosphere reserve: A paradise of biodiversity. *Vaniki Sandesh* **2**(4): 27-37.

Schroeder R, McDonald KC, Chapman BD, Jensen K, Podest E, Tessler ZD and Zimmermann R 2015. Development and evaluation of a multi-year fractional surface water data set derived from active/passive microwave remote sensing data. *Remote Sensing* **7**(12): 16688-16732.

Sekertekin A, Cicekli SY and Arslan N 2018. "Index-Based Identification of Surface Water Resources Using Sentinel-2 Satellite Imagery," *2018 2nd International Symposium on Multidisciplinary Studies and Innovative Technologies,* Ankara, Turkey, pp. 1-5,

Shrestha DP, Saepuloh A and van der Meer F 2019. Land cover classification in the tropics, solving the problem of cloud covered areas using topographic parameters. *International Journal of Applied Earth Observation and Geoinformation* **77**: 84-93.

Sreekanth PD, Krishnan P, Rao NH, Soam SK and Srinivasarao C 2021. Mapping surface-water area using time series landsat imagery on Google Earth Engine: A case study of Telangana, India. *Current Scienc,* **120**(9): 1491-1499.

Tao S, Fang J, Zhao X, Zhao S, Shen H, Hu H and Guo Q 2015. Rapid loss of lakes on the Mongolian Plateau. *Proceedings of the National Academy of Sciences* **112**(7): 2281-2286.

Van der Esch S 2017. Exploring future changes in land use and land condition and the impacts on food, water, climate change and biodiversity: Scenarios for the UNCCD Global Land Outlook, *PBL Netherlands Environmental Assessment Agency* **2076**: 24-71.

Wadhwa A, Santhi K, Kumar KP and Jose J 2018. Identify suitable classification algorithm for water pixel count extraction: A case study of Puzhal Lake. *Indian Journal of Ecology* **45**(4): 697-703.

Wagner PD, Bhallamudi SM, Narasimhan B, Kantakumar LN, Sudheer KP, Kumar S and Fiener P 2016. Dynamic integration of land use changes in a hydrologic assessment of a rapidly developing Indian catchment. *Science of the Total Environment* **539**: 153-164.

Wang Y, Li Z, Zeng C, Xia GS and Shen H 2020. An urban water extraction method combining deep learning and Google Earth engine. *IEEE Journal of Selected Topics in Applied Earth Observations and Remote Sensing* **13**: 769-782.

Watts JD, Kimball JS, Jones LA, Schroeder R and McDonald KC 2012. Satellite Microwave remote sensing of contrasting surface water inundation changes within the Arctic–Boreal Region. *Remote Sensing of Environment* **127**: 223-236.

Xu H 2006. Modification of normalised difference water index (NDWI) to enhance open water features in remotely sensed imagery. *International Journal of Remote Sensing* **27**(14): 3025-3033.

Yang Y, Liu Y, Zhou M, Zhang S, Zhan W, Sun C and Duan Y 2015. Landsat 8 OLI image-based terrestrial water extraction from heterogeneous backgrounds using a reflectance homogenization approach. *Remote Sensing of Environment* **171:** 14-32.

Yang X, Zhao S, Qin X, Zhao N and Liang L 2017. Mapping of urban surface water bodies from Sentinel-2 MSI imagery at 10 m resolution via NDWI-based image sharpening. *Remote Sensing* **9**(6): 596.

Received 22 August, 2023; Accepted 11 February, 2024